Received: 16 May 2024 | Accepted: 26 September 2024

DOI: 10.1002/jmv.29954

RESEARCH ARTICLE

JOURNAL OF MEDICAL VIROLOGY WILEY

Functional evaluation of *TMEM176B* and its predictive role for severe respiratory viral infection through integrated analysis of single-cell and bulk RNA-sequencing

Congcong Shang[1,2] | Jiapei Yu[2] | Shumei Zou[3] | Hui Li[2] | Bin Cao[1,2,4,5] | for the CAP-China network

[1]Graduate School of Peking Union Medical College, Chinese Academy of Medical Sciences & Peking Union Medical College, Beijing, China

[2]National Center for Respiratory Medicine; State Key Laboratory of Respiratory Health and Multimorbidity; National Clinical Research Center for Respiratory Diseases; Institute of Respiratory Medicine, Chinese Academy of Medical Sciences; Department of Pulmonary and Critical Care Medicine, Center of Respiratory Medicine, China-Japan Friendship Hospital, Beijing, China

[3]National Institute for Viral Disease Control and Prevention, Collaborative Innovation Center for Diagnosis and Treatment of Infectious Diseases, Key Laboratory for Medical Virology, Chinese Center for Disease Control and Prevention, Beijing, China

[4]Tsinghua University-Peking University Joint Center for Life Sciences, Tsinghua University, Beijing, China

[5]Department of Pulmonary and Critical Care Medicine, Clinical Center for Pulmonary Infections, Capital Medical University, Beijing, China

Correspondence

Bin Cao, Graduate School of Peking Union Medical College, Chinese Academy of Medical Sciences & Peking Union Medical College, Beijing, China.
Email: caobin_ben@163.com

Hui Li, National Center for Respiratory Medicine; State Key Laboratory of Respiratory Health and Multimorbidity; National Clinical Research Center for Respiratory Diseases; Institute of Respiratory Medicine, Chinese Academy of Medical Sciences; Department of Pulmonary and Critical Care Medicine, Center of Respiratory Medicine, China-Japan Friendship Hospital, Beijing 100029, China.
Email: lihui123000@126.com

Funding information

National Natural Science Foundation of China, Grant/Award Number: 82030002/H0104

Abstract

Transmembrane protein 176B (TMEM176B), localized mainly on the endosomal membrane, has been reported as an immune regulatory factor in malignant diseases. However, the biological function of this molecule remains undetermined during respiratory viral infections. To investigate the functions and prognostic value of this gene, six gene sets were selected from the Gene Expression Omnibus database for research. First, the function of *TMEM176B* and its co-expressed genes were evaluated at different levels (cell, peripheral blood, lung tissue). Afterwards, a machine learning algorithm was utilized to analyze the relationship between *TMEM176B* and its interacting genes with prognosis. After importance evaluation and variable screening, a prognostic model was established. Finally, the reliability of the model was further verified through external data sets. In vitro experiments were conducted to validate the function of *TMEM176B*. *TMEM176B* and its co-expressed genes are involved in multiple processes such as inflammasome activation, myeloid immune cell development, and immune cell infiltration. Machine learning further screened 27 interacting gene modules including *TMEM176B* as prognostic models for severe respiratory viral infections, with the area under the ROC curve (AUCs) of 0.986 and 0.905 in derivation and external validation sets, respectively. We further confirmed that viral load as well as NLRP3 activation and cell death were significantly enhanced in *TMEM176B*$^{-/-}$ THP-1-differentiated macrophages via in vitro experiments. Our study revealed that *TMEM176B* is involved in a wide range of biological functions in respiratory viral infections and has potential prognostic value, which is expected to

Congcong Shang and Jiapei Yu contributed equally to this study.

bring new insights into the clinical management of severe respiratory viral infection hosts.

KEYWORDS
monocytes/macrophages, prognostic model, severe influenza and SARS-CoV-2, *TMEM176B*

1 | INTRODUCTION

Respiratory viruses represented by influenza and SARS-CoV-2, which are highly contagious and pathogenic, pose a great threat to the whole world. There are approximately 3–5 million cases of severe influenza each year, characterized by hypoxemia, respiratory failure and even viral sepsis.[1,2] The COVID-19 pandemic resulted in a decline in global life expectancy by 1–6 years.[3] Although it is currently believed that immune dysfunction and an inflammatory cytokine storm are involved in the pathogenesis of severe influenza, the specific mechanism is still largely unknown. Previous studies have found even after clearing the virus, the immune response that has already been out of control in the body continues to exist, leading to immunopathology and the progression of severe illness.[4,5] Individual genetic background and immune heterogeneity are the basis of different responses to foreign antigens, which can partially explain the varying degrees of immune responses and the final outcome in disease severity. Therefore, it is crucial to identify host factors in the pathogenesis of severe viral pneumonia.

Transmembrane protein 176B (TMEM176B) is a member of the MS4A family, with myeloid immune cell expression specificity and located in the membranes of endosomal systems.[6,7] Studies have revealed that its main functions include maintaining the immature state and promoting the antigen cross-presentation function of dendritic cells.[7,8] Moreover, TMEM176B participates in the pathogenesis of multiple types of malignant diseases by influencing tumor cell proliferation, migration, angiogenesis[9–11] and the inflammatory tumor microenvironment as well as tumor related macrophage (TAM) differentiation.[12–14] TMEM176B is also associated with the occurrence of neurological diseases such as Meniere's disease and cerebellar ataxia.[15,16]

Existing research on TMEM176B mainly focuses on neoplastic diseases and central nervous system diseases. There is limited research available investigating this molecule in infectious diseases. A recent Mendelian randomization analysis suggested significant differential expression patterns of TMEM176B in the peripheral blood of patients with all-cause acute respiratory distress syndrome (ARDS) compared to healthy controls.[17] Furthermore, the expression of TMEM176B in peripheral blood mononuclear cells of COVID-19 pneumonia patients was found to be lower than that of the control group without pneumonia.[18] These observations indicate that this gene may also play a critical role in infectious diseases. However, its specific function in respiratory viral infection remains unclear.

This study aims to investigate the biological role of this molecule during respiratory influenza or SARS-CoV-2 infection and explore its potential as a biomarker for predicting disease severity and prognosis. Considering the distinct immune phenotypes between the circulating peripheral blood and lungs, we initially selected and analyzed public datasets comprising primary cells, peripheral blood samples, and lung tissue. Subsequently, we utilized various bioinformatics algorithms to comprehensively explore the involvement of *TMEM176B* in multiple biological processes from different perspectives. Based on these findings, we further investigated its interacting molecules to analyze their potential prognostic value in severe viral pneumonia cases. Finally, functional validation was conducted by constructing a *TMEM176B*$^{-/-}$ THP-1 cell line.

2 | MATERIALS AND METHODS

2.1 | Data source

To study the molecular interactions of the *TMEM176B* in different types of samples, six gene sets from the Gene Expression Omnibus database (http://www.ncbi.nlm.nih.gov/gds/) were selected for the study.[19–24] Details of the datasets involved are listed in Table S1. Classic and widely studied genes related to inflammasomes and pyroptosis were collected for correlation analysis.[25–27] Inflammasome-related genes: *NLRC4*, *NLRP1*, *NLRP2*, *NLRP3*, *NLRP6*, *NLRP7*, *NOD1*, *NOD2*, *PLCG1*, *PRKACA*, *PYCARD*, *SCAF11*, *TIRAP*, *TNF* (Table S2). Pyroptosis-associated genes: *AIM2*, *CASP1*, *CASP3*, *CASP4*, *CASP5*, *CASP6*, *CASP8*, *CASP9*, *ELANE*, *GPX4*, *GSDMA*, *GSDMB*, *GSDMC*, *GSDMD*, *IL-18*, *IL-1B*, *IL-6* (Table S3). All data was analyzed with R 4.3.1.

2.2 | Overall technical route

TMEM176B was evaluated at cellular, pulmonary, and hematological levels, respectively (Figure S1). Single-cell analysis and annotation were achieved through Package Seurat 4.4.0 (https://satijalab.org/seurat/) and Package SingleR 2.4.0 (https://github.com/dviraran/SingleR). At the cellular level, the infected cell samples of GSE97672 were selected for Weighted Gene Co-expression Network (WGCNA) analysis (Package WGCNA 17.2-1, https://horvath.genetics.ucla.edu/html/CoexpressionNetwork/Rpackages/WGCNA/), then the correlation between each clustering module and inflammasome-pyroptosis related genes was analyzed. For the hematological level, the samples with infection from peripheral blood in GSE149689 were screened and dimensionality reduction clustered, then myeloid cells were selected from the infection samples for high dimensional WGCNA

(hdWGCNA) and pseudo-temporal analysis (Package hdWGCNA 0.2.24, https://smorabit.github.io/hdWGCNA/articles/basic_tutorial.html). Correlation analysis was performed between each clustering module and genes related to inflammasome-pyroptosis. GSE163959 was selected for the pulmonary level, with the samples of infected patients selected for WGCNA and immune infiltration analysis. Subsequently, correlation analysis was performed between each clustering module and inflammasome-pyroptosis-related genes as well as the abundance of immune cells.

The value of *TMEM176B* in predicting prognosis in hosts with influenza A virus infection was evaluated as follows. (1) GSE202001 (mouse lung tissue). After selecting infected samples, cell screening and dimensionality reduction clustering were performed, followed by hdWGCNA analysis and pseudotime series analysis (Package monocle 2.30.0, https://cole-trapnell-lab.github.io/monocle-release/) in myeloid cells. Correlation analysis was performed between each clustering module and the inflammasome-pyroptosis-related genes. Then genes unrelated to inflammasomes were excluded to obtain *Tmem176b* co-expressed as well as inflammasome-related gene module; Pseudo-temporal analysis was performed to obtain *Tmem176b* co-expression gene module related with cell differentiation. Afterward, by taking the intersection of the above modules, we obtained a module that is related to both inflammasomes and cell differentiation. Human homologous genes were translated and further analyzed with prognosis using machine learning algorithms. (2) GSE157344 (human BALF). After selecting all patient samples through cell screening and dimensionality reduction clustering, macrophages were screened, and cell clustering was performed using the K-nearest neighbor (KNN) algorithm to obtain machine-learning samples. The samples were divided into training and validation sets, with prognosis as the outcome variable and the module gene obtained in the previous step as the feature value. After importance evaluation and variable screening, a prognosis model was established. (3) GSE145926 (human BALF). After selecting samples from infected patients and conducting cell screening and dimensionality reduction clustering, macrophages were screened, and cell clustering was performed using the KNN algorithm to obtain machine-learning samples. These samples were used as external validation sets to validate the trained model.

2.3 | Construction of co-expressed gene modules

The WGCNA method was used for GSE97672 and GSE163959. The WGCNA R software package was used to construct and modularize different gene networks. The FPKM of the samples was organized into clusters to identify any potential significant outliers that may exist. Then, an automated network system was utilized to establish a co-expression network. Two methods were adopted for the module: hierarchical clustering and dynamic truncation function detection. The connections between the module and various phenotypes were established, and analyzed by the correlation between the module eigengene (ME) values and expression levels of inflammasomes and pyroptosis-related genes, as well as the abundance of immune cells. The abundance of immune cells was obtained through immune infiltration analysis using CIBERSORT.

2.4 | scRNA-seq data processing and pseudo-temporal analysis

We conducted quality control and processed all datasets (GSE149689, GSE202001, GSE157344, GSE145926) individually using Seurat. Following read count normalization with 'LogNormalize', we performed principal component analysis (PCA), uniform manifold approximation and projection (UMAP), as well as shared nearest neighbors clustering on the data. Cell type annotation of clusters was accomplished using SingleR and manual annotation utilizing cell type markers. Trajectory analysis was applied to GSE163959 and GSE202001 using Monocle 2. After estimating size factors and gene expression dispersion with estimateSizeFactors and estimate dispersions, respectively, dimension reduction was performed on the normalized count matrix using the DDRTree algorithm-based reduceDimension function with default parameters.

Subsequently, ordering cells and conducting differential gene testing allowed us to identify cellular timing-related genes. Finally, branched expression analysis modeling (BEAM) was employed for trajectory branching analysis to identify differentiation-related genes.

2.5 | RNA velocity analysis

We performed RNA rate analysis using the scVelo package.[28] ScVelo employs a dynamics model based on likelihood estimation to quantify the comprehensive dynamics of transcriptional events, encompassing both mRNA splicing and non-splicing dynamics, on a per-gene basis. By employing RNA velocity analysis, transient cellular states within the data set can be effectively identified and characterized, while also providing insight into the future progression of transcriptome features along the trajectory of cellular recognition. These projections are derived from gene-specific estimates of mRNA transcription, splicing, and degradation rates, enabling the estimation of the relative position of each cell within its own potential differentiation process. Finally, the RNA velocity of all genes is projected onto the arrow represented on the UMAP plot.

2.6 | Pathway analysis

We performed Gene Set Enrichment Analysis using the enrichGO and enrichKEGG functions in the R package clusterProfiler. To understand the biological relevance of the module discovered through the GSE202001 data set analysis, we tested the significance of the over-representation of genes reflected in Gene Ontology (GO) annotation and KEGG pathway and adjusted the p-values from the test using the Benjamini–Hochberg method.

2.7 | Establishment of machine learning model

Macrophages from the GSE157344 and GSE145926 datasets were selected and clustered using the KNN algorithm to obtain

440 and 479 samples, respectively. The prognosis of all individuals was obtained and used as the response variable, with a poor prognosis assigned as 0 and a good prognosis assigned as 1. As for GSE157344, patients in the data set were all ICU severe cases. We classified deceased cases as having a poor prognosis and surviving patients as having a good prognosis. In the GSE145926, infected patients were involved and prognostic values were assigned based on the severity of symptoms, as it is generally believed that patients with severe symptoms have a worse prognosis than those with mild symptoms. The 440 samples in GSE157344 were divided into training and validation sets in a 6:4 ratio. The gene expression levels in the modules discovered through the GSE202001 data set analysis were used as feature values for the classifier, and the Random Forest model was used for training. Subsequently, the importance ranking of feature variables was performed. MeanDecreaseGini values below 0.3 were considered unrelated to prognosis, so they were removed, and the model was retrained using the remaining variables. Finally, the trained model was applied to the 479 sample of GSE145926 for external validation.

2.8 | Cells, viruses, and chemical reagents

MDCK cells were cultured in Dulbecco's Modified Eagle's Medium and THP-1 (Procell Life Science & Technology) cell lines were cultured in ATCC-modified 1640 supplemented with high glucose and L-glutamine (Gibco®) in addition to 10% fetal bovine serum and 1% penicillin/streptomycin in a 5% CO_2 incubator at 37°C. All cells used are routinely tested for mycoplasma and are maintained mycoplasma-free. Mouse-adapted virus strain A/Puerto Rico/8/34 (H1N1) was grown in allantoic cavities from 10 to 11-day-old fertile chicken eggs for 2 days at 37°C. Plaque assay was performed to determine the titer of the virus.

THP-1 monocytes were differentiated into macrophages by treatment with 100 ng/mL PMA (Sigma) for 48 h. A *TMEM176B*$^{-/-}$ THP-1 cell strain was constructed using the CRISPR/Cas9 system from Jiman Biotechnology company. Lipopolysaccharide (LPS) and Nigericin were purchased from Sigma and Selleck, respectively.

2.9 | Influenza virus infection and inflammasome activation

THP-1 differentiated macrophages were incubated with the influenza virus at an MOI = 10 in 200 μL/well of 0.1% bovine serum albumin–phosphate-buffered saline (PBS) at 1 × 106 cells/12-well plate for 1.5 h, washed thoroughly, and incubated in complete media for an additional 24 h according to the experimental design. LPS-primed (100 ng/mL, 4 h) THP-1 differentiated macrophages treated with nigericin (20 μM) for 45 min were used as the positive control. The cell-free supernatant was collected and analyzed for IL-1β by enzyme-linked immunosorbent assay (ELISA) and western blot analysis. Cell lysates were also collected for western blot analysis.

2.10 | ELISA

The concentration of IL-1β in the cell supernatant was measured with a mouse IL-1β ELISA kit (NeoBioscience) according to the manufacturer's instructions (Tecan).

2.11 | RNA extraction and quantitative polymerase chain reaction (qPCR)

The total RNAs were extracted with the RNeasy Mini Kit (Qiagen). RNA quantity and quality were assayed using a Nanodrop 2000 spectrophotometer (Thermo Fisher Scientific). A two-step method was used for qPCR using the RevertAid First Strand cDNA Synthesis Kit (Thermo Fisher Scientific) and the applied biosystems PowerUp™ SYBR™ Green Master Mix (Thermo Fisher Scientific). Primers used for the qPCR were as follows: *HA*: forward (5'−3'), GCCCAACCACAACACAAA; reverse (5'−3'), GCCCTCCTTCTCCGTCAG. *NP*: forward (5'−3'), AGCCTAATCAGACC AAAT; reverse (5'−3'), ACCTGCTTCTCAGTTCAA. *GAPDH*: forward (5'−3'), TGTGAACCATGAGAAGTATG; reverse (5'−3'), TTCCACGATA CCAAAGTTGT.

2.12 | Western blot analysis

Cells were washed once in PBS and lysed in cell lysis buffer (Applygen) containing phenylmethylsulfonyl fluoride. Cell lysates were clarified by centrifugation, separated by SDS-PAGE, and transferred to a PVDF membrane (Beyotime FFP24). Membranes were blocked in QuickBlock buffer (Beyotime P0252) for 30 min at room temperature before incubation with the indicated antibodies overnight at 4°C. After three washes with TBST (Servicebio G0004), the membranes were incubated with the corresponding secondary antibodies for 1 h at room temperature. Protein bands were visualized by chemiluminescence reagent according to the manufacturer's instructions (NCM Biotech P2100).

To detect the secretion of IL-1βp17, the cell culture supernatants were concentrated by TCA protein precipitation kit (C510011, Sangon Biotech), according to the manufacturer's instructions. Then IL-1βp17 (R&D Systems) was detected by Western blot analysis.

2.13 | Flow cytometry

Caspase-1 activation was determined using the FLICA pyroptosis detection kit for Caspase-1 (Immunochemistry Technologies) according to the manufacturer's guidelines. Fluorescence was evaluated by flow cytometry using CytoFLEX LX V5-B4-R3 instruments (Beckman Coulter Life Sciences). Data were analyzed using FlowJo software (version 10.8.1).

2.14 | Statistics

Pearson correlation analysis was used to determine correlations, with $p < 0.05$ indicating significant relevance. Experimental values are presented as mean ± SD of individual samples. One-way analysis of variance or Student's *t* test was performed to assess statistical significance based on the characteristics of the data using GraphPad Prism 9.0. $p < 0.05$ was considered statistically significant.

3 | RESULTS

3.1 | *TMEM176B* with its co-expressed gene modules is closely related to the expression of inflammasome-pyroptosis genes

To investigate the biological processes in which *TMEM176B* is involved, we conducted research based on multiple datasets. Infected samples from GSE97672 (human primary monocytes) and GSE163959 (respiratory tissue) were selected for WGCNA analysis (Figure S2A,B). Through hierarchical clustering analysis and dynamic branch cut methods for gene dendrograms, genes were grouped into 16 modules and 30 modules and TMEM176B was found in the green and turquoise modules which included 334 and 842 genes, respectively (Figure 1A,C). In GSE97672, the green module is significantly associated with inflammasome-pyroptosis-related genes such as *NLRP2*, *NLRP3*, *NOD1*, *NOD2*, *TIRAP*, *AIM2*, *GPX4*, *GSDMB*, *GSDMD*, *IL6* (Figure 1B). In GSE163959, the turquoise module is also closely linked to *NLRP4*, *NLRP1*, *NOD1*, *NOD2*, *TIRAP*, *TNF*, *CASP3*, *CASP8*, *GSDMB*, *GSDMC*, *IL6* (Figure 1D).

GSE149689 is a single-cell RNA sequencing data set of peripheral blood from influenza-infected patients. The KNN algorithm was used to reduce the sparsity of the expression matrix in myeloid cells (monocytes, macrophages, neutrophils), and a total of 378 meta cells were clustered with 10 selected as the soft thresholding power β to ensure a biologically significant scale-free network (Figure S2C). After selecting influenza-infected samples and performing dimensionality reduction clustering, the distribution of cell types is shown in Figure S2D. *TMEM176B* is exclusively expressed in monocytes and macrophages (Figure S2E). Through hierarchical clustering analysis

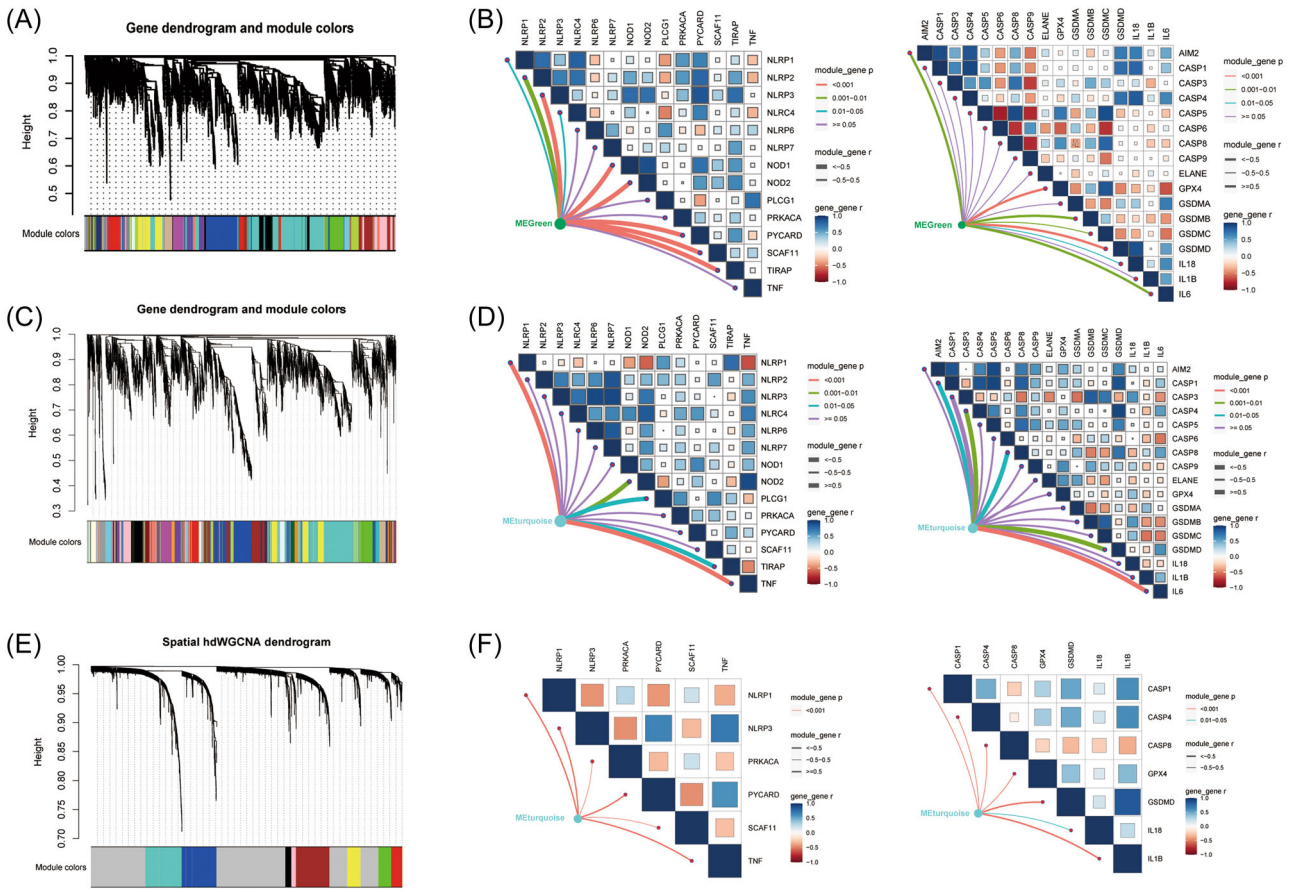

FIGURE 1 Relationship of *TMEM176B* and its co-expressed gene module with inflammasome-pyroptosis genes. (A) Weighted Gene Co-expression Network (WGCNA) analysis of GSE97672. (B) The Green module of GSE97672, which includes *TMEM176B*, is related to inflammasome-pyroptosis-related genes. (C) WGCNA analysis of GSE163959. (D) The Turquoise module of GSE163959, which includes *TMEM176B*, is related to inflammasome-pyroptosis-related genes. (E) hdWGCNA of GSE149689. (F) The Turquoise module of GSE149689, which includes *TMEM176B*, is associated with inflammasome-pyroptosis-related genes.

and dynamic branch-cut methods for gene dendrograms, the genes were grouped into 8 modules (Figure 1E). *TMEM176B* is located in the turquoise module which includes 672 genes, and shows a good correlation with *NLRP1*, *NLRP3*, *PRKACA*, *PYCARD*, *SCAF11*, *TNF*, *CASP1*, *CASP4*, *CASP8*, *GPX4*, *GSDMD*, *IL18*, *IL1B* (Figure 1F). Collectively, these results indicate that *TMEM176B* may participate in inflammasome activation and pyroptosis.

3.2 | *TMEM176B* is involved in the infiltration of immune cells in respiratory tissue

Abundance of immune cells in the lung was analyzed with GSE163959 (Figure 2A). Correlation analysis between each infiltrated immune cell type and the turquoise module, which includes *TMEM176B* was performed. The turquoise module is positively related to plasma cells, regulatory T cells (Treg), T follicular helper cells (Tfh), dendritic cell (DC) activation, and resting mast cells, while it is negatively related to M0/M2-state macrophages, mast cell activation and neutrophil infiltration (Figure 2B). This suggests *TMEM176B* may be involved in the regulation of both innate and adaptive immune responses.

3.3 | *TMEM176B* takes part in cell development and differentiation of myeloid cells

Pseudo-temporal analysis for myeloid cells was performed with GSE149689 (peripheral blood) and GSE202001 (mouse lung tissue) data set. Cell pseudo-temporal diagrams and temporal expression changes of TMEM176B were revealed (Figure 3A,B). *TMEM176B* increases with the maturation of cells in peripheral blood, while increases first, then decreases in lung tissue (Figure 3C,D). To strengthen the findings pertaining to discrepancies in gene expression patterns, we conducted RNA velocity analysis on the datasets GSE149689 (Figure S3A) and GSE202001 (Figure S3B). We identified the top50 dynamical genes along with latent time including *TMEM176B* (Figure S3C,S3D). Furthermore, we graphically illustrate the changes in gene expression, with the horizontal axis representing the latent time calculated by RNA rates and the vertical axis indicating the gene expression level within single cells. The color scheme utilized in the graph signifies the temporal progression of each individual cell (Figure S3E,S3F). The results also displayed diverse expression patterns alongside the trajectory of cellular differentiation, likely reflecting the presence of cell heterogeneity within distinct immune compartments After performing temporal differential gene analysis, it was found that the *TMEM176B* is a developmental temporal-related gene both in peripheral blood and lung tissue (Figure 3E,G). Branch trajectory prediction shows that myeloid cells mainly differentiate into two subtypes in peripheral blood and lung tissue. Main differentiation nodes were selected and the BEAM function was used for calculation. The results show that *TMEM176B* is related to the differentiation direction of myeloid cells in peripheral blood and lung tissue (Figure 3F,H). Taken together, *TMEM176B* may participate in the developmental and differentiation processes of myeloid cells and have a certain impact on immune homeostasis.

3.4 | *TMEM176B* with its interacting genes in macrophages could be used to predict the prognosis of patients with respiratory viral infections

The distribution of cell types in GSE202001 (mouse lung tissue) is shown after dimensionality reduction clustering (Figure 4A). We utilized the KNN algorithm to co-aggregate class metacells, selected a soft threshold of 6 (Figure S4A), and constructed the TOM matrix. With hierarchical clustering analysis and dynamic branch cut methods for gene dendrograms, genes were grouped into 9 modules (Figure S4B). *Tmem176b* is located in the turquoise module including 1795 genes and its relationship with inflammasome-pyroptosis genes is shown (Figure S4C). To describe the interaction between genes and phenotype, module membership (MM) and gene significance (GS)

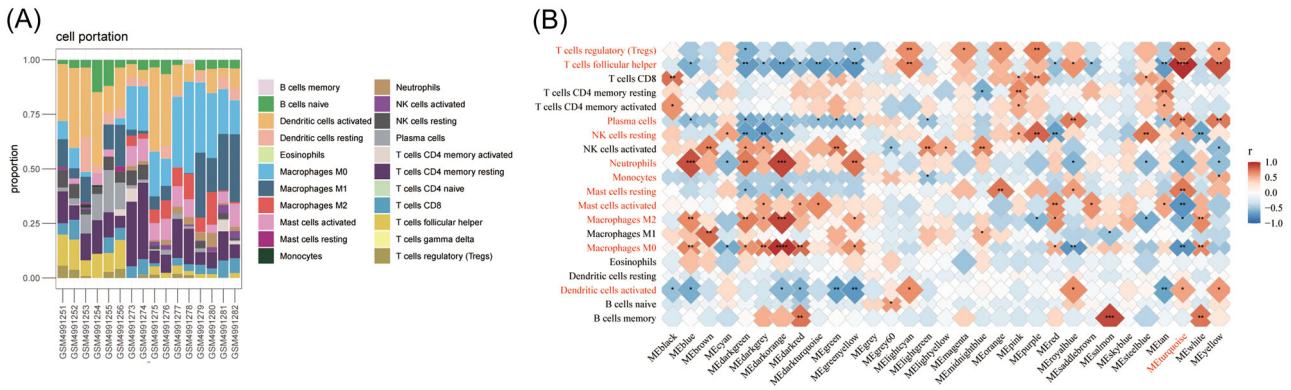

FIGURE 2 Immune cell infiltration analysis in GSE163959. (A) Abundance of immune cells in each sample collected from individuals infected with influenza infection. (B) Correlation analysis between each infiltrated immune cell and different gene modules, especially the one including *TMEM176B*.

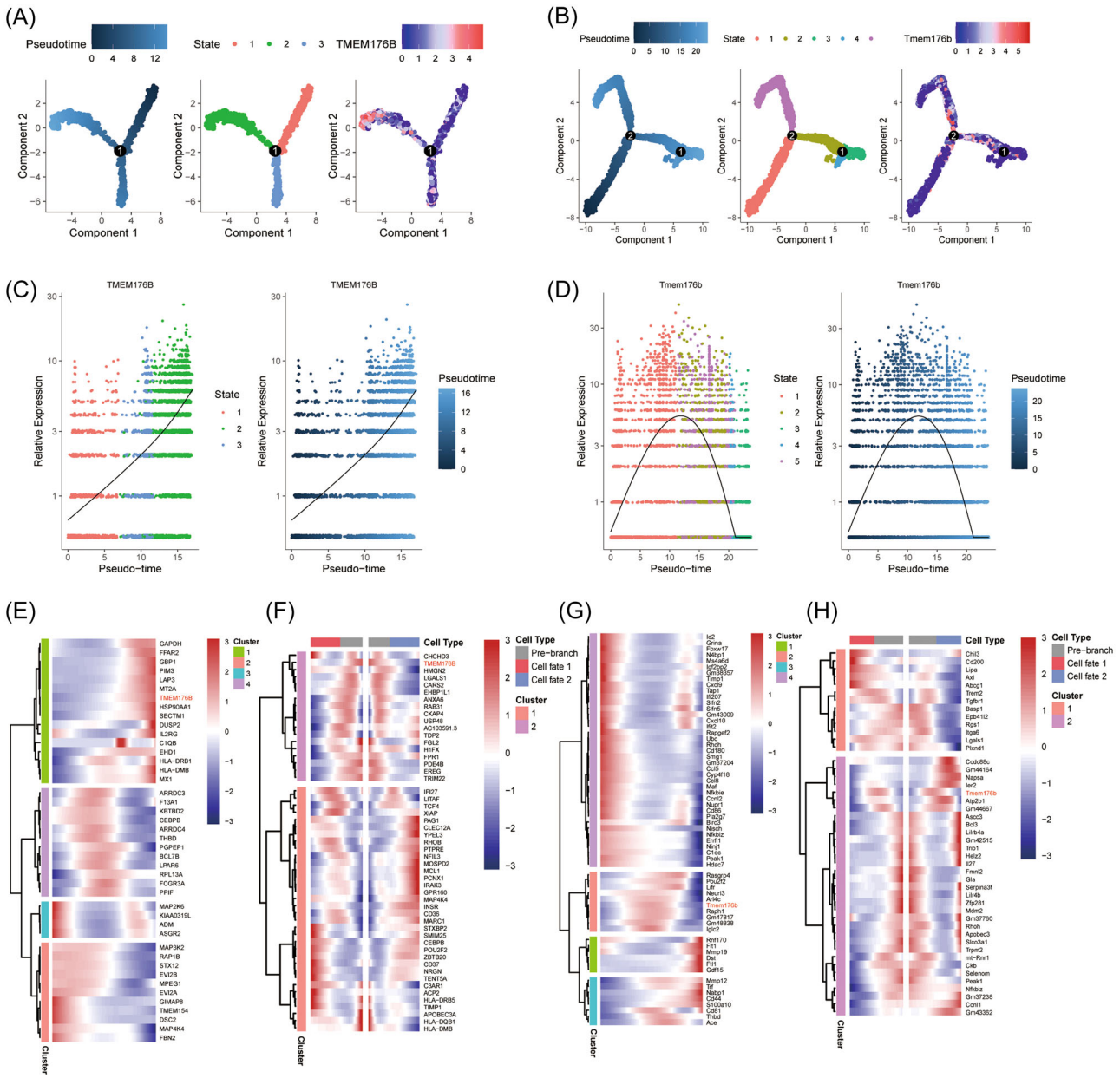

FIGURE 3 Pseudo-temporal analysis for myeloid cells of GSE149689 (peripheral blood) and GSE202001 (lung tissue). (A, C) Cell pseudo-temporal diagrams and *TMEM176B* temporal expression changes in GSE149689. (B, D) Cell pseudo-temporal diagrams and *TMEM176B* temporal expression changes in GSE202001. (E, G) Temporal differential gene analysis in GSE149689 (E) and GSE202001 (G). (F, H) Branch trajectory prediction analysis in GSE149689 (F) and GSE202001 (H).

were calculated and shown (Figure 4B). GS, a term in WGCNA, represents the correlation coefficient between each gene's expression level and its phenotype values (Pearson correlation), reflecting the correlation between gene expression and phenotype. We use *p*-GS to denote its statistical significance, and only 2 genes were excluded with *p*-GS < 0.05. Additionally, genes with a correlation value below 0.1 with the GS were further excluded. Ultimately, a total of 1778 molecules were obtained in the module related to inflammasome gene (NLRP3 module) (Figure 4B). Differentiation-related genes obtained from the pseudo-temporal analysis were clustered with "ward. D2"resulted in a total of 483 molecules in the differentiation module, which includes *Tmem176b* (differentiation module). By taking the intersection of the above two modules, a total of 185 *Tmem176b* co-expression molecules were obtained, which are involved in two biological processes (*NLRP3* and differentiation module) (Figure 4C; Tables S4 and S5). Then enrichment analysis of the gene module was performed. GO analysis verified that these genes were mainly involved in macrophage activation, myeloid cell differentiation, phagocytosis, early endosome, immune receptor activity, MAP kinase tyrosine phosphatase activity which are related to inflammation and cell differentiation (Figure 4D). KEGG analysis revealed that these genes were also involved in inflammation and cell differentiation

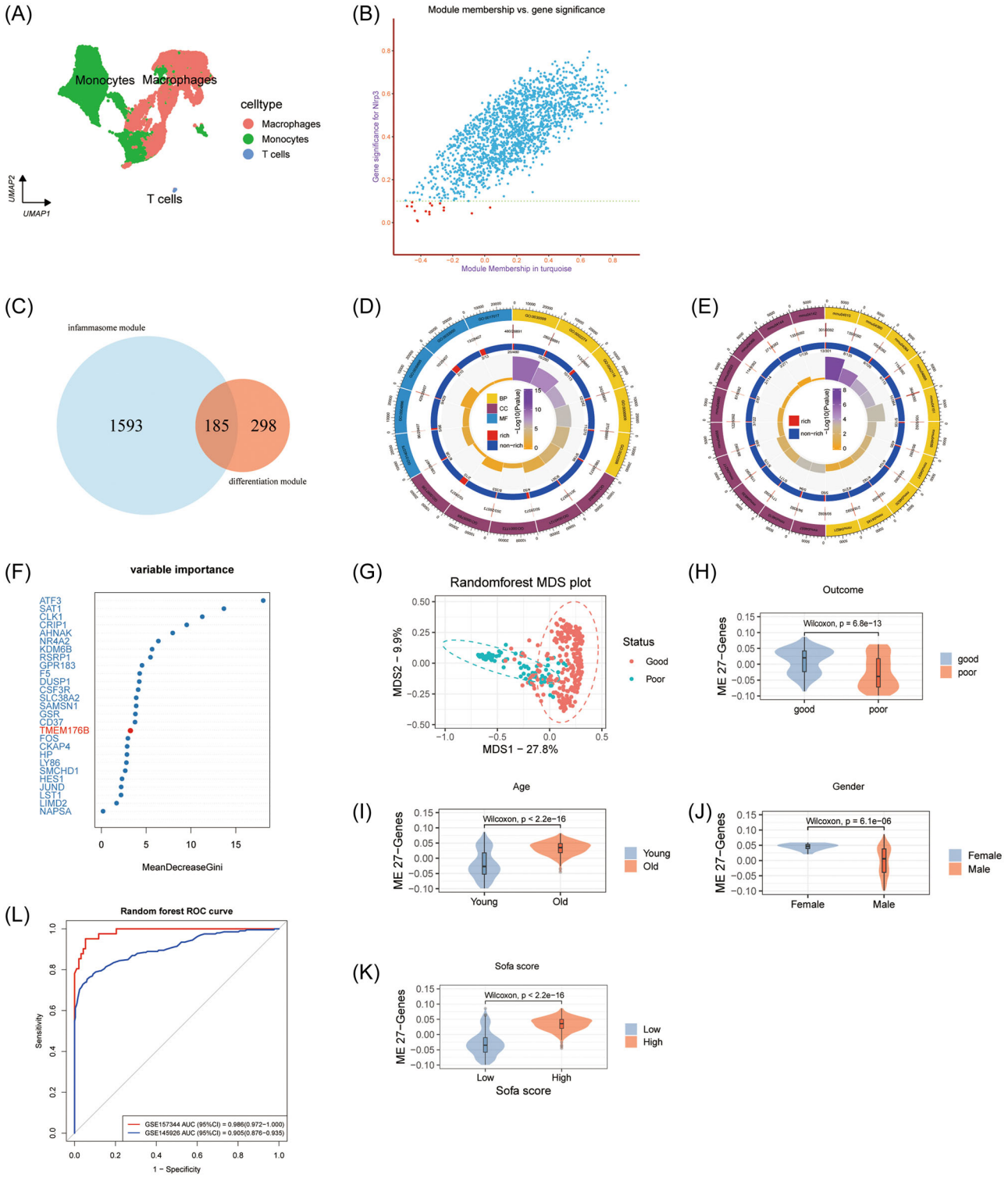

FIGURE 4 Establishment of prognostic model by *TMEM176B* and its related genes. (A) Clustering of GSE202001. (B) Gene significance <0.1 was chosen to delete little correlated molecules with NLRP3. (C) Venn diagrams indicate overlap of 185 *TMEM176B* co-expression genes involved NLRP3 and differentiation module. (D, E) Gene Ontology (GO) and Kyoto Encyclopedia of Genes and Genomes (KEGG) analysis of 185 genes. (F–H) Random Forest model was used in the training set of GSE157344 to obtain 27 genes which affect prognosis (H, Wilcoxon test, $p < 0.05$). (I–K) Distinct expression pattern of ME values of 27 genes in related to age (cut-off 65), gender, and sofa score (cut-off 5) (Wilcoxon test, $p < 0.05$). (L) Receiver-operator characteristic (ROC) curves of GSE157344 and GSE145926.

pathways such as MAPK, NF-kappa B, NOD-like receptor signaling pathway, TNF signaling pathway, Toll-like receptor signaling pathway, complement and coagulation cascades, Th1/Th2 and Th17 cell differentiation as well as Phagosome, Lysosome, Endocytosis that related to the endomembrane system (Figure 4E). These results above reflect the potential regulatory involvement of *Tmem176b* in immune response, so we speculate that this gene may affect prognosis and further establish a prognostic model.

The *NLRP3* and differentiation module analyzed above were transformed into human homologous genes, resulting in 148 genes including *TMEM176B*. The Random Forest model was used to evaluate the importance of variables in the training set of GSE157344, and variables that did not contribute to the model were deleted. Finally, 27 genes in which *TMEM176B* MeanDecreaseGini value is 3.19 were obtained as well as a Random Forest MDS plot, indicating the interaction between *TMEM176B* and its related molecules can predict prognosis (Figure 4F–H). Moreover, the first principal component of 27 genes expression level was compared in different clinical features, and it was found that the expression patterns were distinct in different ages, genders, and SOFA scores (Wilcoxon test, $p < 0.05$) (Figure 4I–K). Twenty-seven molecules were selected for further training and the prognostic model was obtained with area under the ROC curve (AUC) values of 1 and 0.986 under the ROC curve in the training and internal validation set, respectively (Figure 4L). Then external validation of the model was performed in GSE145926 with an AUC of 0.905 under the ROC curve (Figure 4L). The first principal component of 27 gene expression patterns in GSE157344 and GSE145926 were shown (Figure 5SA,S5B). This evidence indicates that *TMEM176B* may be a reliable biomarker for predicting the outcome of patients with respiratory viral infection.

3.5 | In vitro validation of the regulatory role of *TMEM176B* in inflammasome activation and viral load during influenza A virus infection

Based on the analysis above, we further validated the regulatory effect of *TMEM176B* on NLRP3 activation in vitro using THP-1 cells. THP-1 cells, with or without *TMEM176B*, were differentiated into macrophages and subsequently infected with influenza A virus in vitro. Flow cytometry was employed to assess the activation level of caspase-1, while the proportion of pyroptotic cells was determined using caspase-1/PI double staining. Enhanced caspase-1 activation and cell death in *TMEM176B* knockout cells were observed (Figures 5A,B and S6). Accordingly, IL-1β secreted in the cell supernatant using ELISA showed a significant increase in *TMEM176B* knockout cells (Figure 5C) and further supported by cleaved IL-1β in the cell supernatant detected by immunoblotting (Figure 5D). These results all confirm that *TMEM176B* is a molecule that regulates the activation of inflammasome.

Given that viral load is a critical determinant of overactivated inflammation and disease prognosis, we further tested the viral load in THP-1 differentiated macrophages with or without *TMEM176B*. Both mRNA levels of HA and NP were significantly higher in *TMEM176B* knockout cells compared to wildtype cells (Figure 5E). In conclusion, *TMEM176B* may serve as a host protective marker involved in viral clearance and the limitation cell inflammation and death.

4 | DISCUSSION

We conducted a comprehensive evaluation of the crucial biological processes associated with *TMEM176B* at the transcriptome level during respiratory viral infection, encompassing various sample types such as cells, peripheral blood, and lung tissue for the first time. Our findings demonstrated that *TMEM176B* plays a significant role in the activation of inflammatory responses, facilitating immune cell infiltration and differentiation. Consequently, it can be concluded that this gene is closely related to the immune response after virus infection, and shows reliable value in predicting the adverse outcomes of respiratory viral infectious diseases. We also confirmed *TMEM176B* deletion promotes inflammasome activation, cell death and viral replication in vitro. These results provide valuable insights for further investigations into the potential role of *TMEM176B* in the clinical management of severe viral infectious diseases.

Overactivation of NLRP3 and the increased release of inflammatory factors contribute to cytokine storm formation and immunopathology, leading to the progression of severe viral pneumonia.[29–32] Previous studies have found small molecule inhibitors of TMEM176B and PD-1/PD-L1 immune checkpoint inhibitors work synergistically to enhance antitumor immunity and improve prognosis.[13] The underlying mechanism is that inhibition of TMEM176B transforms the tumor microenvironment from a "cold tumor" to a "hot tumor" state. In addition, the pro-inflammatory effect of CD146 positive macrophages is also related to the inhibition of TMEM176B expression.[12] These studies have both suggested that TMEM176B may possess a regulatory role in inflammatory activation. However, it remains unclear whether its molecular function in the tumor microenvironment is also applicable to infection scenarios, considering the distinct nature of inflammation induced by live viral particles.

In addition, intervention treatments also differ, because the mechanism behind the occurrence and development of tumors is an immunosuppressive microenvironment, while severe respiratory virus infection is characterized by a hyperactive immune response and inflammation. Appropriate anti-inflammatory treatment can be beneficial for severe respiratory virus infection.[33,34] To explore whether this molecule is involved in the regulation of inflammatory activation during respiratory virus infection and its potential intervention value, we first analyzed the relationship between *TMEM176B* and inflammasome-pyroptosis-related genes at the transcriptome level from multiple datasets. Our findings demonstrated that in the context of influenza virus infection, *TMEM176B* and its co-expressed genes exhibited significant associations with the activation of inflammasome-pyroptosis genes in primary cells, peripheral blood, and lung tissues.

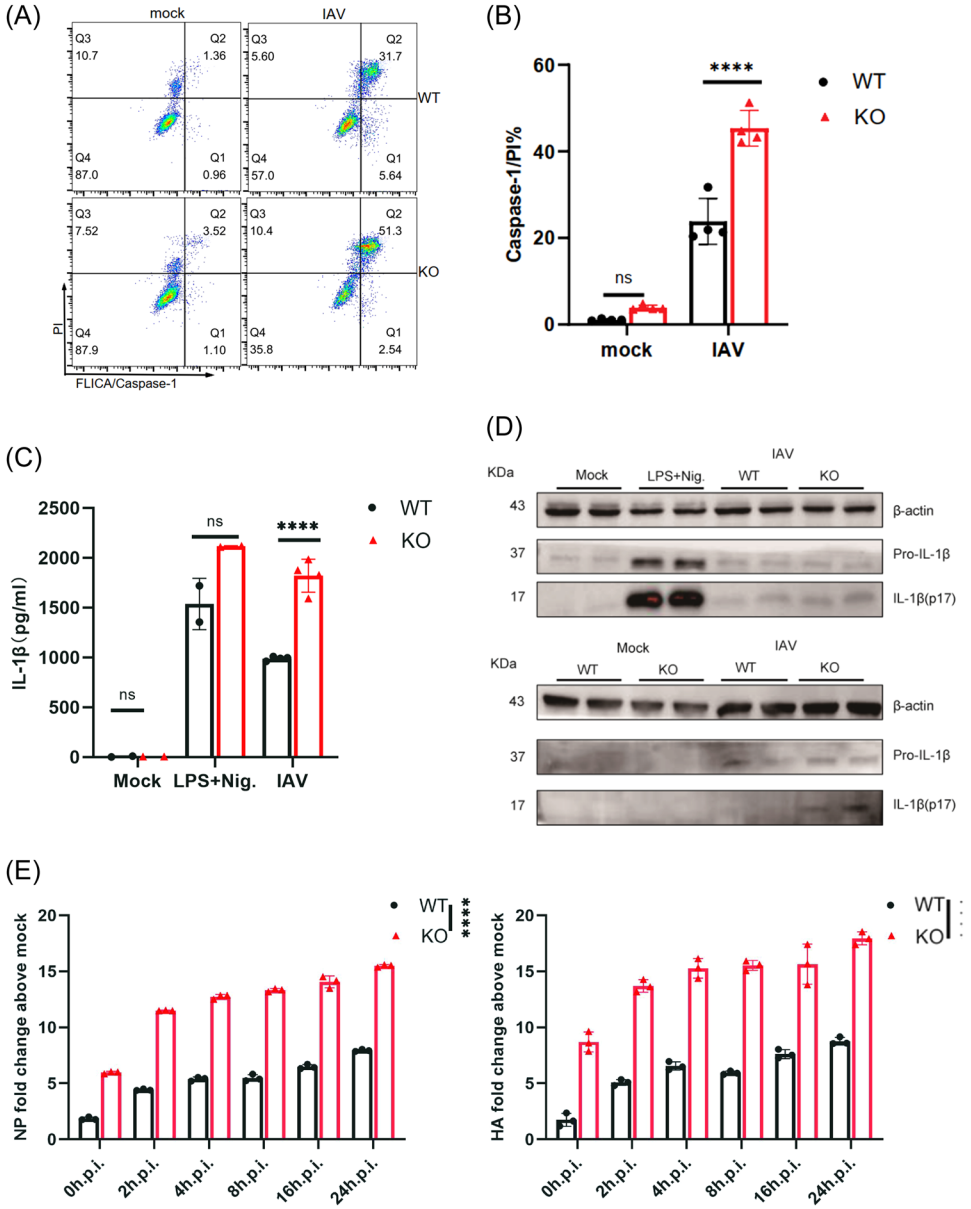

FIGURE 5 In vitro functional verification of TMEM176B. (A, B) Caspase-1/PI double staining of THP-1 differentiated macrophages infected with IAV. (C) IL-1β (pg/mL) in cell supernatant tested by enzyme-linked immunosorbent assay (ELISA). (D) Immunoblotting analysis of cleaved IL-1β in the cell supernatant. (E) Influenza copies in THP-1 differentiated macrophages with or without TMEM176B at 0–24 h.p.i. points over time. Student *t* test was performed. ns, not significant, $^{*}p < 0.05$, $^{**}p < 0.01$, $^{***}p < 0.001$, $^{****}p < 0.0001$. Data are presented as mean ± SD.

Considering that the activation of inflammasomes is a multifactorial and multi-step process,[35,36] and the regulation of this process may not only occur at the transcriptional level, the correlation of *TMEM176B* with inflammasomes analyzed by bioinformatics is not sufficient. Then we further confirmed this through THP-1-induced macrophages in vitro viral infection experiment. NLRP3 activation is enhanced in *TMEM176B* knock-out macrophages, verifying its role in participating in the regulation of the inflammatory response in influenza. Recent studies have found that interruption of intracellular vesicle transport is a prerequisite for NLRP3 activation,[37–39] and intracellular acidification is a key factor in maintaining normal intracellular transport.[40,41] TMEM176B, an ion channel protein located on the inner membrane, plays a crucial role in regulating pH homeostasis within organelles and consequently modulating vesicle transport kinetics.[8] We speculate that the involvement of this protein in NLRP3 activation may be related to changes in the aforementioned biological processes.

Additionally, it is widely acknowledged that the viral load plays a crucial role in determining the prognosis. A previous study has demonstrated that inflammasome activation in infected macrophages contributes to COVID-19 pathology, indicating that an inability to control viral replication may trigger an aberrant inflammatory response.[42] Our findings also indicate that the absence of TMEM176B leads to an increased viral load, which could provide another explanation for

excessive inflammasome activation. In conclusion, this research highlights the significant involvement of TMEM176B in influenza infection. However, further validation through animal experiments is still required.

Initially, we planned to perform developmental trajectory analysis using both peripheral blood and lung tissue samples. However, due to the unavailability of a single-cell data set for influenza infection in human lung tissue, we opted to utilize the GSE202001 mouse data set instead. Our analysis revealed that *TMEM176B* exhibits associations with cell development and differentiation in monocyte-macrophages in both peripheral blood and lung tissues. However, the temporal expression of *TMEM176B* in peripheral blood and lung tissue is different. The expression level of *TMEM176B* in peripheral blood increased with cell maturation, while a trend of first increasing and then decreasing in lung tissues was found. This discrepancy was also validated by the RNA velocity analysis of this gene. We speculate that it may derive from cell heterogeneity due to distinct immune compartments.[43,44] However, this does not affect our conclusion that *TMEM176B* undertakes potential functions in cell differentiation and development. Inconsistency with a previous study, *TMEM176B* decreases in dendritic cells derived from bone marrow as the cells mature.[7] We postulate that the role of this molecule in developmental trajectories may vary across different cell types, necessitating further validation through future experimental investigations. However, it is unequivocal that this molecule is intricately associated with distinct differentiation pathways of myeloid immune cells in both peripheral blood and lung tissue. Moreover, diverse cellular differentiation states are closely intertwined with cell functionality, inflammatory response intensity, and even disease prognosis.[24,45] M1/M2 macrophages are the two main subtypes of differentiated states, and the homeostasis of M1/M2 macrophages determines the trend of inflammation expansion and resolution.[46,47] A large number of studies have shown that the excessive infiltration of M1 macrophages is one of the main reasons for severe viral pneumonia. M1 macrophages have stronger pro-inflammatory effects than M2, and are conducive to the intracellular replication and release of COVID-19.[47,48] *TMEM176B* is involved in the direction of cell differentiation and may serve as a molecular determinant of disease progression by fine-tuning the development and differentiation of myeloid immune cells. In addition, we also conducted immune infiltration analysis with data set from lung tissue samples and found that *TMEM176B* and its interacting genes were positively correlated with the degree of infiltration of plasma cells, Treg, activated NK cells, and activated dendritic cells, while negatively correlated with M0 and M2 infiltration, indicating that *TMEM176B* affects disease prognosis via shaping the lung immune environment.

Based on the analysis above, we hold the opinion that *TMEM176B* is closely related to immune processes and speculate that this gene has potential prognostic value. Furthermore, in the GSE202001 dataset, we identified a module that includes *TMEM176B*, and is involved in both inflammasome activation and cell differentiation. GO and KEGG enrichment analyses suggest that this gene module is closely related to the activation and differentiation of immune cells, as well as inflammatory response processes. These biological processes are important events in antiviral infection and are closely related to patient prognosis. Therefore, we conducted an analysis of patient prognosis. Given the limited prognostic information available in single-cell data of the influenza A virus, we incorporated COVID-19-related data into our study, as it can induce similar immunological responses observed in severe diseases. The GSE157344 was divided into a training set and a validation set, and after machine learning training, 27 molecules including *TMEM176B* were finally identified as prognostic markers. The powerful prognostic predictive effect was further validated through an external validation set. As is well known, age and SOFA score are exact risk factors for severe viral pneumonia.[2] Differences in immune response mediated by sex hormones make women more resistant to the virus than men.[49] The principal component analysis of our prognostic model also revealed distinct expression patterns in populations with different clinical characteristics mentioned above, which align consistently with the clinical features of severe viral pneumonia and underscore its robust predictive capability.

In summary, we conducted a comprehensive data analysis of the function of *TMEM176B* in viral infections for the first time and validated its prognostic significance. *TMEM176B* exhibits potential as a host regulatory factor and holds promise as an intervention target for severe infectious diseases.

AUTHOR CONTRIBUTIONS

Bin Cao and Hui Li supervised and revised the manuscript. Congcong Shang and Jiapei Yu designed the study and performed the experiments, data collection, and data analysis. Congcong Shang wrote the original draft. Jiapei Yu and Shumei Zou edited the manuscript. All authors contributed to the article and approved the submitted version.

ACKNOWLEDGMENTS

The authors thank everyone who contributed to the public data set used in this study. This study is supported by the CAMS Institute of Respiratory Medicine Grant for Young Scholars [grant No. 2023-ZF-17], National Natural Science Foundation of China [grant No. 82030002/H0104].

CONFLICT OF INTEREST STATEMENT

The authors declare no conflict of interest.

DATA AVAILABILITY STATEMENT

The datasets generated during or analyzed during the current study are publicly available. The data underlying this article will be shared upon reasonable request to the corresponding author.

REFERENCES

1. Wei X, Narasimhan H, Zhu B, Sun J. Host recovery from respiratory viral infection. *Annu Rev Immunol*. 2023;41:277-300.
2. Flerlage T, Boyd DF, Meliopoulos V, Thomas PG, Schultz-Cherry S. Influenza virus and SARS-CoV-2: pathogenesis and host responses in the respiratory tract. *Nat Rev Microbiol*. 2021;19(7):425-441.
3. GBD 2021 Demographics Collaborators. Global age-sex-specific mortality, life expectancy, and population estimates in 204 countries and territories and 811 subnational locations, 1950-2021, and the

impact of the COVID-19 pandemic: a comprehensive demographic analysis for the global burden of disease study 2021. *The Lancet*. 2024;403(10440):1989-2056.
4. Thomas PG, Dash P, Aldridge JR, et al. The intracellular sensor NLRP3 mediates key innate and healing responses to influenza A virus via the regulation of caspase-1. *Immunity*. 2009;30(4):566-575.
5. Major J, Crotta S, Llorian M, et al. Type I and III interferons disrupt lung epithelial repair during recovery from viral infection. *Science*. 2020;369(6504):712-717.
6. Louvet C, Chiffoleau E, Heslan M, et al. Identification of a new member of the CD20/FcεRIβ family overexpressed in tolerated allografts. *Am J Transplant*. 2005;5(9):2143-2153.
7. Condamine T, Le Texier L, Howie D, et al. Tmem176B and Tmem176A are associated with the immature state of dendritic cells. *J Leukoc Biol*. 2010;88(3):507-515.
8. Segovia M, Louvet C, Charnet P, et al. Autologous dendritic cells prolong allograft survival through Tmem176b-dependent antigen cross-presentation. *Am J Trans*. 2014;14(5):1021-1031.
9. Ryu SH, Kim KH, Kim HB, et al. Oncogenic ras-mediated down-regulation of Clast1/LR8 is involved in ras-mediated neoplastic transformation and tumorigenesis in NIH3T3 cells. *Cancer Sci*. 2010;101(9):1990-1996.
10. Yang Y, Feng Q, Hu K, Cheng F. Using CRISPRa and CRISPRi technologies to study the biological functions of ITGB5, TIMP1, and TMEM176B in prostate cancer cells. *Front Mol Biosci*. 2021;8:676021.
11. Kang C, Rostoker R, Ben-Shumel S, et al. TMEM176B regulates AKT/mTOR signaling and tumor growth in triple-negative breast cancer. *Cells*. 2021;10(12):3430.
12. Jing L, An Y, Cai T, et al. A subpopulation of CD146(+) macrophages enhances antitumor immunity by activating the NLRP3 inflammasome. *Cell Mol Immunol*. 2023;20(8):908-923.
13. Segovia M, Russo S, Jeldres M, et al. Targeting TMEM176B enhances antitumor immunity and augments the efficacy of immune checkpoint blockers by unleashing inflammasome activation. *Cancer Cell*. 2019;35(5):767-781.e6.
14. Li Z, Zhou B, Zhu X, et al. Differentiation-related genes in tumor-associated macrophages as potential prognostic biomarkers in non-small cell lung cancer. *Front Immunol*. 2023;14:1123840.
15. Sun Y, Zhang D, Sun G, et al. RNA-sequencing study of peripheral blood mononuclear cells in sporadic ménière's disease patients: possible contribution of immunologic dysfunction to the development of this disorder. *Clin Exp Immunol*. 2018;192(1):33-45.
16. Seki T, Sato M, Kibe Y, et al. Lysosomal dysfunction and early glial activation are involved in the pathogenesis of spinocerebellar ataxia type 21 caused by mutant transmembrane protein 240. *Neurobiol Dis*. 2018;120:34-50.
17. Cao S, Li H, Xin J, et al. Identification of genetic profile and biomarkers involved in acute respiratory distress syndrome. *Intensive Care Med*. 2024;50(1):46-55.
18. Pekayvaz K, Leunig A, Kaiser R, et al. Protective immune trajectories in early viral containment of non-pneumonic SARS-CoV-2 infection. *Nat Commun*. 2022;13(1):1018.
19. Steel J, Lowen AC, Pena L, et al. Live attenuated influenza viruses containing NS1 truncations as vaccine candidates against H5N1 highly pathogenic avian influenza. *J Virol*. 2009;83(4):1742-1753.
20. Alfi O, Yakirevitch A, Wald O, et al. Human nasal and lung tissues infected ex vivo with SARS-CoV-2 provide insights into differential tissue-specific and virus-specific innate immune responses in the upper and lower respiratory tract. *J Virol*. 2021;95(14):e0013021.
21. Lee JS, Park S, Jeong HW, et al. Immunophenotyping of COVID-19 and influenza highlights the role of type I interferons in development of severe COVID-19. *Sci Immunol*. 2020;5(49):eabd1554.
22. Li F, Piattini F, Pohlmeier L, Feng Q, Rehrauer H, Kopf M. Monocyte-Derived alveolar macrophages autonomously determine severe outcome of respiratory viral infection. *Science Immunology*. 2022;7(73):eabj5761.
23. Bost P, De Sanctis F, Canè S, et al. Deciphering the state of immune silence in fatal COVID-19 patients. *Nat Commun*. 2021;12(1):1428.
24. Liao M, Liu Y, Yuan J, et al. Single-cell landscape of bronchoalveolar immune cells in patients with COVID-19. *Nature Med*. 2020;26(6):842-844.
25. Liu A, Shen L, Li N, Shen L, Li Z. Pan-cancer analyses of pyroptosis with functional implications for prognosis and immunotherapy in cancer. *J Transl Med*. 2022;20(1):109.
26. Zou Y, Xie J, Zheng S, et al. Leveraging diverse cell-death patterns to predict the prognosis and drug sensitivity of triple-negative breast cancer patients after surgery. *Int J Surg*. 2022;107:106936.
27. Fu J, Schroder K, Wu H. Mechanistic insights from inflammasome structures. *Nat Rev Immunol*. 2024;24(7):518-535.
28. Bergen V, Lange M, Peidli S, Wolf FA, Theis FJ. Generalizing RNA velocity to transient cell states through dynamical modeling. *Nature Biotechnol*. 2020;38(12):1408-1414.
29. Szabo PA, Dogra P, Gray JI, et al. Longitudinal profiling of respiratory and systemic immune responses reveals myeloid cell-driven lung inflammation in severe COVID-19. *Immunity*. 2021;54(4):797-814.
30. Vora SM, Lieberman J, Wu H. Inflammasome activation at the crux of severe COVID-19. *Nat Rev Immunol*. 2021;21(11):694-703.
31. Morris G, Bortolasci CC, Puri BK, et al. The cytokine storms of COVID-19, H1N1 influenza, CRS and MAS compared. Can one sized treatment fit all? *Cytokine*. 2021;144:155593.
32. Fajgenbaum DC, June CH. Cytokine storm. *N Engl J Med*. 2020;383(23):2255-2273.
33. Jia X, Liu B, Bao L, et al. Delayed oseltamivir plus sirolimus treatment attenuates H1N1 virus-induced severe lung injury correlated with repressed NLRP3 inflammasome activation and inflammatory cell infiltration. *PLoS Pathog*. 2018;14(11):e1007428.
34. Liu B, Bao L, Wang L, et al. Anti-IFN-γ therapy alleviates acute lung injury induced by severe influenza a (H1N1) Pdm09 infection in mice. *J Microbiol Immunol Infect*. 2021;54(3):396-403.
35. Barnett KC, Li S, Liang K, Ting JPY. A 360° view of the inflammasome: mechanisms of activation, cell death, and diseases. *Cell*. 2023;186(11):2288-2312.
36. Xu J, Núñez G. The NLRP3 inflammasome: activation and regulation. *Trends Biochem Sci*. 2023;48(4):331-344.
37. Kagan JC. Excess lipids on endosomes dictate NLRP3 localization and inflammasome activation. *Nature Immunol*. 2023;24(1):3-4.
38. Zhang Z, Venditti R, Ran L, et al. Distinct changes in endosomal composition promote NLRP3 inflammasome activation. *Nature Immunol*. 2023;24(1):30-41.
39. Lee B, Hoyle C, Wellens R, et al. Disruptions in endocytic traffic contribute to the activation of the NLRP3 inflammasome. *Sci Signaling*. 2023;16(773):eabm7134.
40. Chapman RE, Munro S. Retrieval of TGN proteins from the cell surface requires endosomal acidification. *EMBO J*. 1994;13(10):2305-2312.
41. Reaves B, Banting G. Vacuolar ATPase inactivation blocks recycling to the trans-Golgi network from the plasma membrane. *FEBS Lett*. 1994;345(1):61-66.
42. Sefik E, Qu R, Junqueira C, et al. Inflammasome activation in infected macrophages drives COVID-19 pathology. *Nature*. 2022;606(7914):585-593.
43. Xu G, Qi F, Li H, et al. The differential immune responses to COVID-19 in peripheral and lung revealed by single-cell RNA sequencing. *Cell Discov*. 2020;6:73.

44. Gordon S, Taylor PR. Monocyte and macrophage heterogeneity. *Nat Rev Immunol*. 2005;5(12):953-964.
45. Wauters E, Van Mol P, Garg AD, et al. Discriminating mild from critical COVID-19 by innate and adaptive immune single-cell profiling of bronchoalveolar lavages. *Cell Res*. 2021;31(3):272-290.
46. Yao D, Bao L, Li F, et al. H1N1 influenza virus dose dependent induction of dysregulated innate immune responses and STAT1/3 activation are associated with pulmonary immunopathological damage. *Virulence*. 2022;13(1):1558-1572.
47. Wang Z, Li S, Huang B. Alveolar macrophages: Achilles' heel of SARS-CoV-2 infection. *Signal Transduct Target Ther*. 2022;7(1):242.
48. Lv J, Wang Z, Qu Y, et al. Distinct uptake, amplification, and release of SARS-CoV-2 by M1 and M2 alveolar macrophages. *Cell Discov*. 2021;7(1):24.
49. Hoffmann JP, Liu JA, Seddu K, Klein SL. Sex hormone signaling and regulation of immune function. *Immunity*. 2023;56(11):2472-2491.

SUPPORTING INFORMATION

Additional supporting information can be found online in the Supporting Information section at the end of this article.

How to cite this article: Shang C, Yu J, Zou S, Li H, Cao B, for the CAP-China network. Functional evaluation of *TMEM176B* and its predictive role for severe respiratory viral infection through integrated analysis of single-cell and bulk RNA-sequencing. *J Med Virol*. 2024;96:e29954. doi:10.1002/jmv.29954